Supporting Information

Synchronously introducing and encasing non-stoichiometric defects in TiO_2 nanowires by NEG coating and interface reconstruction for sustainable photoelectrochemical water oxidation

Feifei Guo,[a] *Yan Wang,*[a] *Haibo Shu,*[a] *Zhijie Wang,*[a] *Jiaping Liu,*[a] *Yun Cai,*[a] *Jun Fang*[a] *and Yang Yang*[*a]

[a] State Key Laboratory of Materials-Oriented Chemical Engineering, College of Chemical Engineering, Nanjing Tech University, Nanjing 211816, China

*Email: yangy@njtech.edu.cn

Supplementary experimental section

Preparation of TiO_2 thin films by magnetron sputtering

TiO_2 thin film was coated on the cleaned FTO glass using radio-frequency magnetron sputtering for 3 h. Prior to deposition, the chamber was evacuated to a base pressure below 1.0×10^{-2} Pa. High-purity Ar (99.99%) was introduced at a flow rate of 40 sccm, and the working pressure was maintained at 3.0×10^{-2} Pa. The TiO_2 target was pre-sputtered with Ar plasma for 10 min to remove surface impurities. During sputtering, the substrate rotation speed was set to 8 rpm, and the sputtering power was fixed at 80 W.

Preparation of reduced TiO_2 thin films by Ti NEG coating and direct chemical reduction

Reduced TiO_2 thin films were prepared by the same protocols as described in the main text for TiO_2 NWAs. The resulting samples through Ti NEG coating reduction and direct chemical reduction are designated as TiO_2 film@Ti-3-N and TiO_2 film-V_o, respectively.

Supplementary Figures

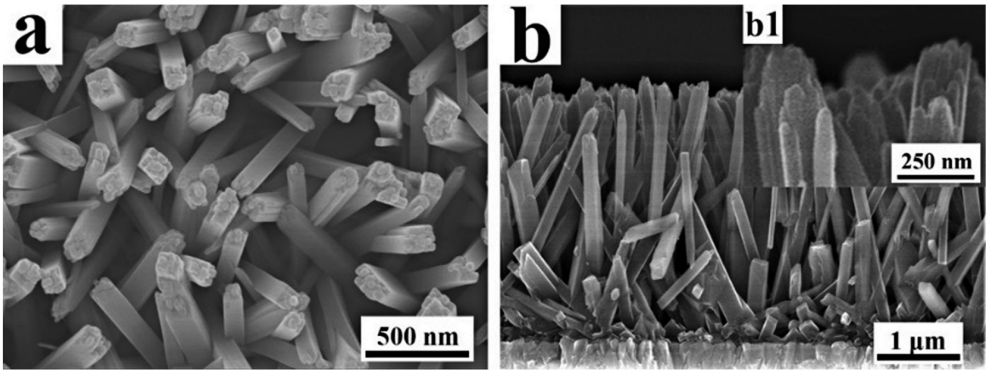

Fig. S1. SEM images of TiO_2@Ti-3 grown on the FTO substrate: (a) top view, and (b) cross-sectional view. (b1) in the inset of (b) is a magnified cross-sectional view.

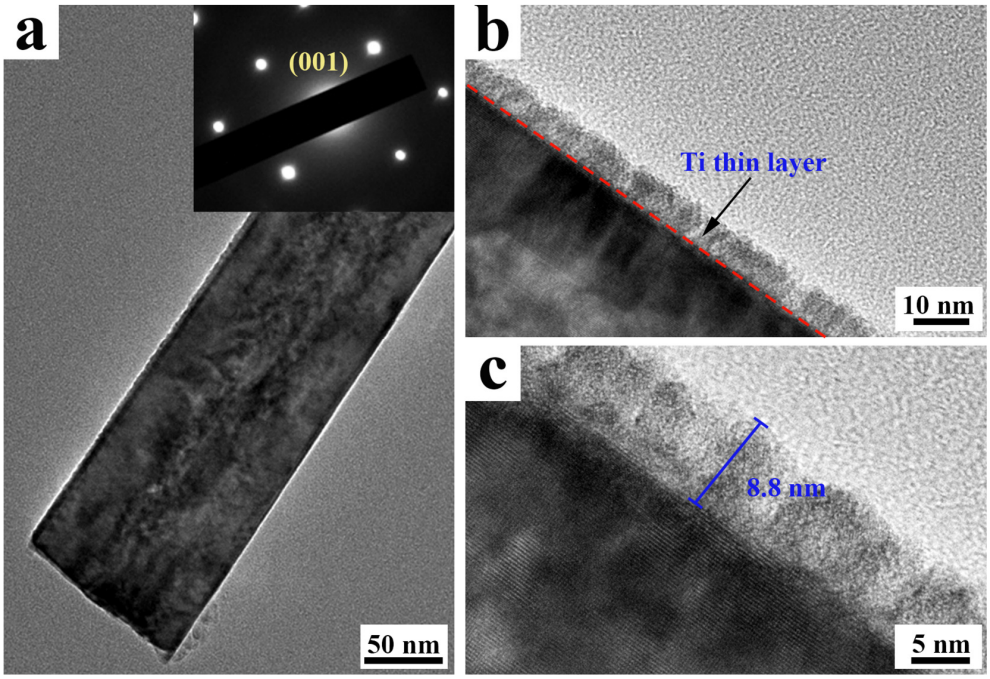

Fig. S2. (a) TEM images of TiO_2@Ti-3; the inset in the upper right is the corresponding SAED pattern. (b, c) High-resolution TEM images.

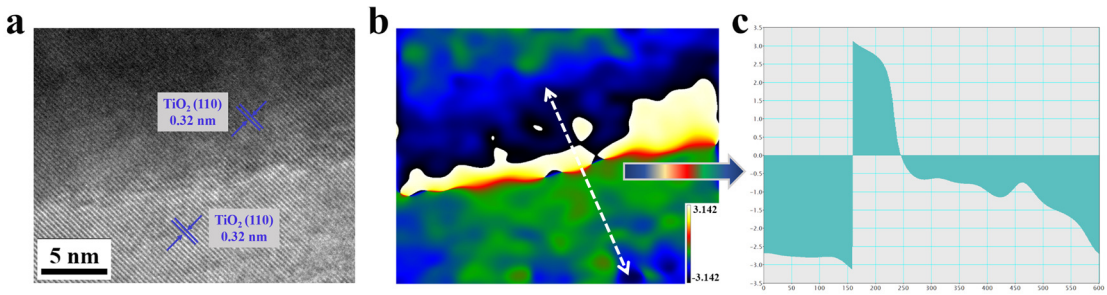

Fig. S3. (a) High-resolution TEM image showing the core–shell interface of TiO_2@Ti-3-N. (b) Corresponding GPA strain distribution map and (c) normal-strain profile along the white dashed line in (b).

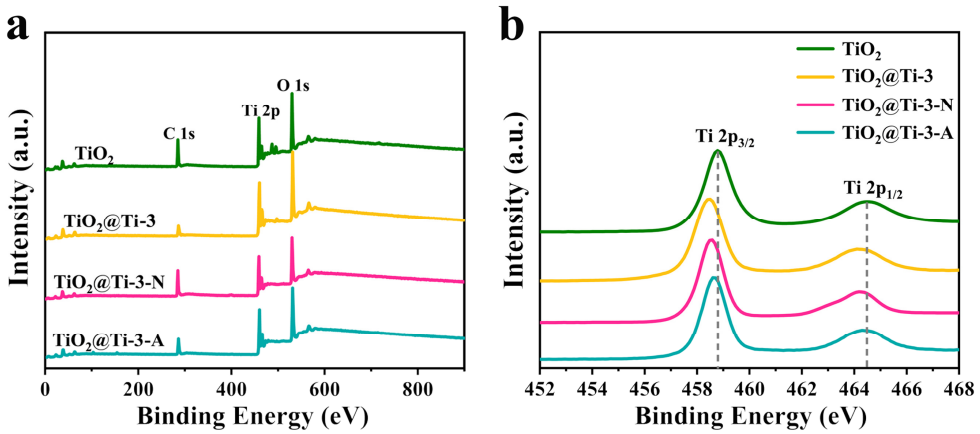

Fig. S4. (a) XPS survey spectra and (b) XPS Ti 2p spectra of TiO_2, TiO_2@Ti-3, TiO_2@Ti-3-N and TiO_2@Ti-3-A.

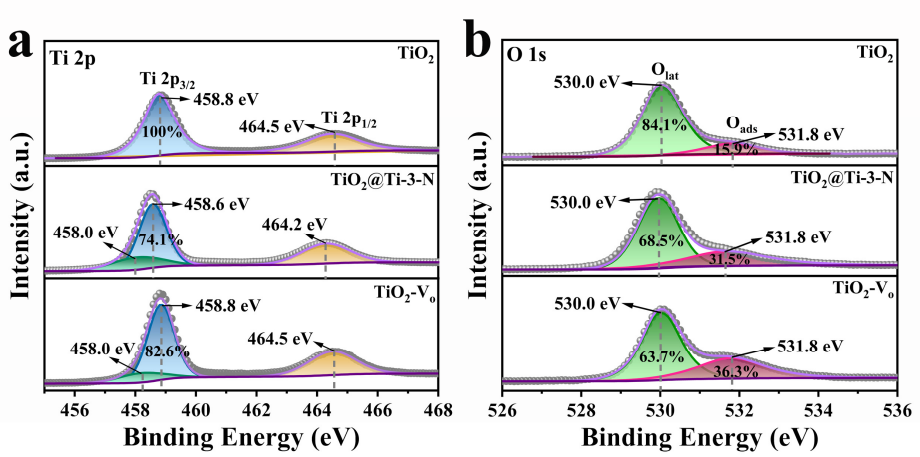

Fig. S5. High-resolution XPS spectra of Ti 2p (a) and O 1s (b) of TiO_2, TiO_2@Ti-3-N and TiO_2-V_o.

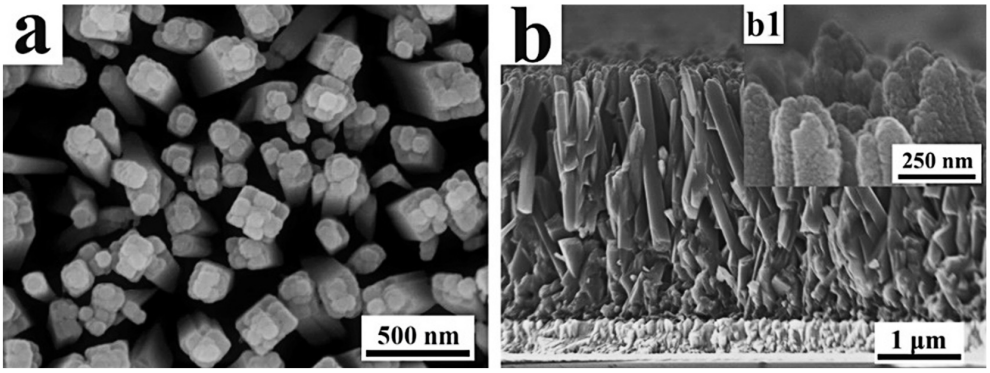

Fig. S6. SEM images of TiO_2@Ti-9-N grown on the FTO substrate: (a) top view, and (b) cross-sectional view. (b1) in the inset of (b) is a magnified cross-sectional view.

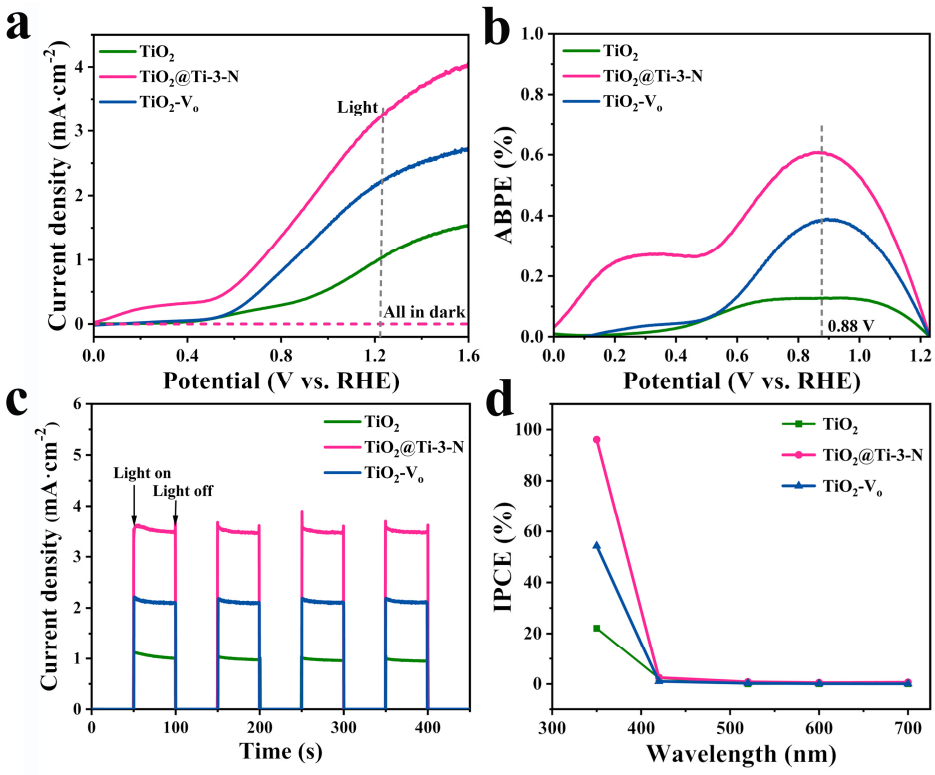

Fig. S7. PEC performance of TiO_2, TiO_2@Ti-3-N and TiO_2-V_o: (a) LSV plots measured in dark and under full-spectrum light illumination (100 mW·cm^{-2}), (b) ABPE curves, (c) amperometric *J*–*t* curves measured at a bias of 1.23 V vs. RHE under chopped light illumination, and (d) IPCE curves.

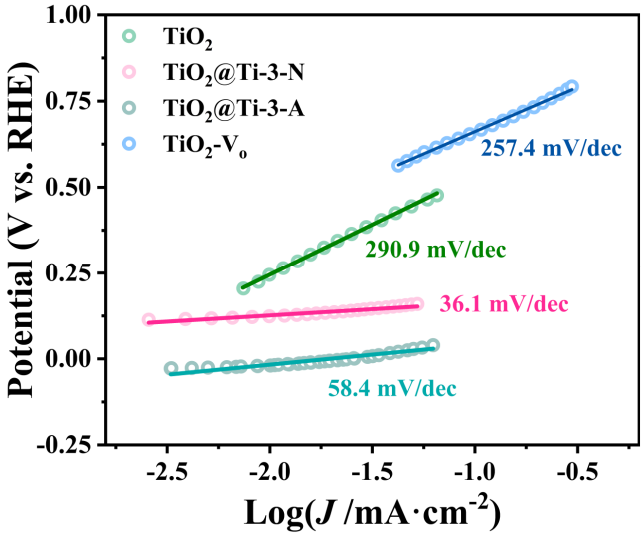

Fig. S8. Tafel plots of TiO_2, TiO_2@Ti-3-N, TiO_2@Ti-3-A and TiO_2-V_o measured under full-spectrum light illumination (100 mW·cm^{-2}).

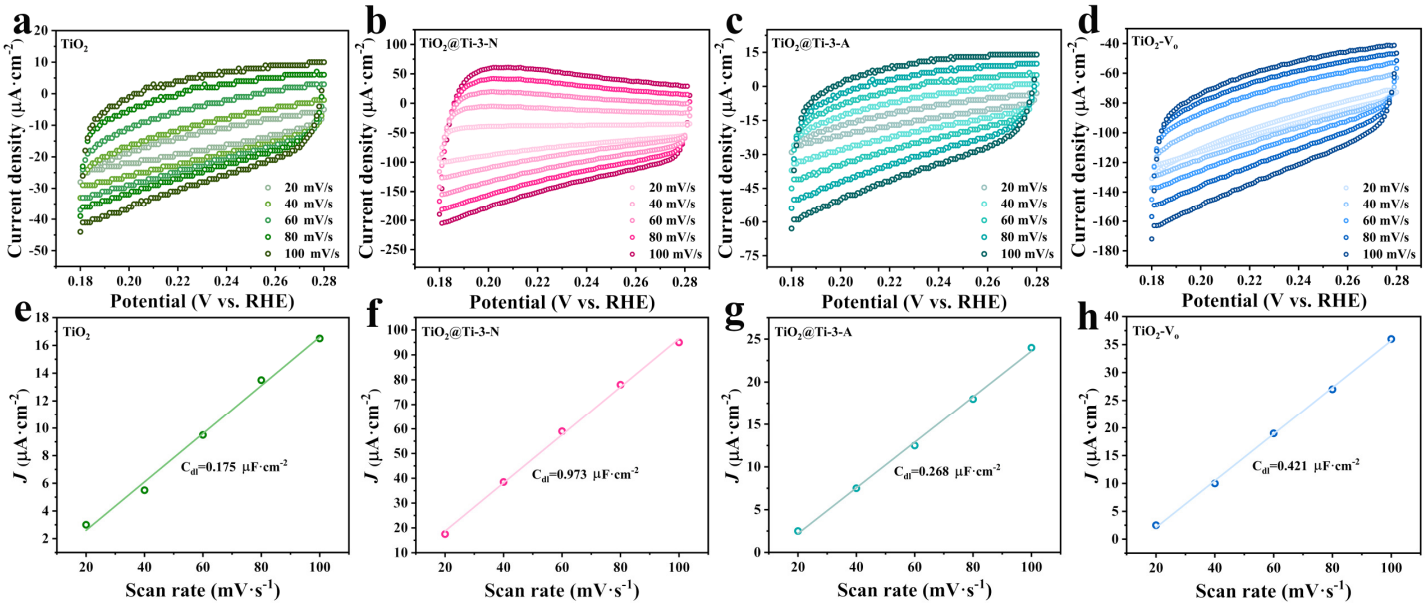

Fig. S9. (a–d) CV curves recorded at different scan rates in the non-faradaic capacitance current range in 0.5 M Na_2SO_4 electrolyte solution. (e–h) Corresponding capacitive current differences at 0.23 V vs. RHE as a function of scan rate among TiO_2, TiO_2@Ti-3-N, TiO_2@Ti-3-A and TiO_2-V_o.

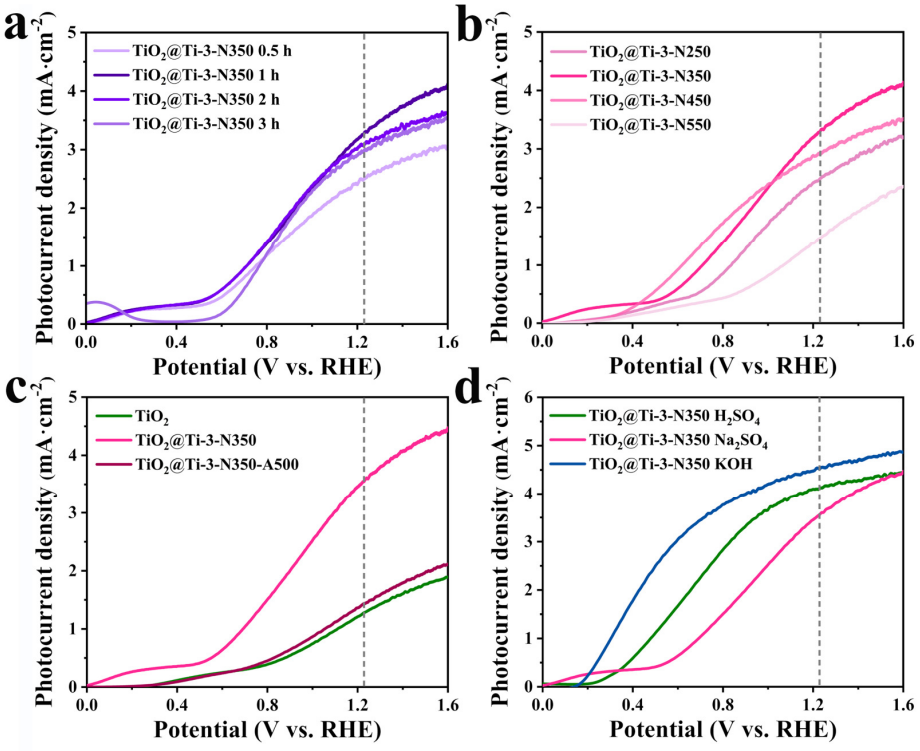

Fig. S10. LSV plots of TiO_2 photoanodes measured under full-spectrum illumination (100 mW·cm^{-2}): (a) TiO_2@Ti-3-N prepared by different annealing time, (b) TiO_2@Ti-3-N prepared by different annealing temperatures, (c) TiO_2@Ti-3-N treated with a secondary annealing at 500 ºC in air, and (d) TiO_2@Ti-3-N in different electrolytes.

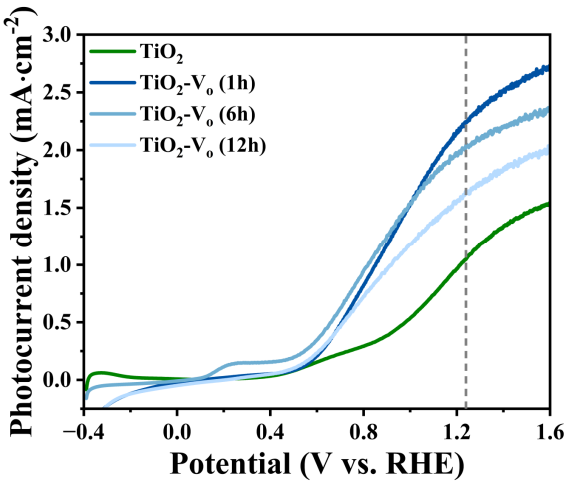

Fig. S11. LSV plots measured under full-spectrum light illumination (100 mW·cm^{-2}) of TiO_2 photoanodes treated with 0.5 M $NaBH_4$ solution for different time.

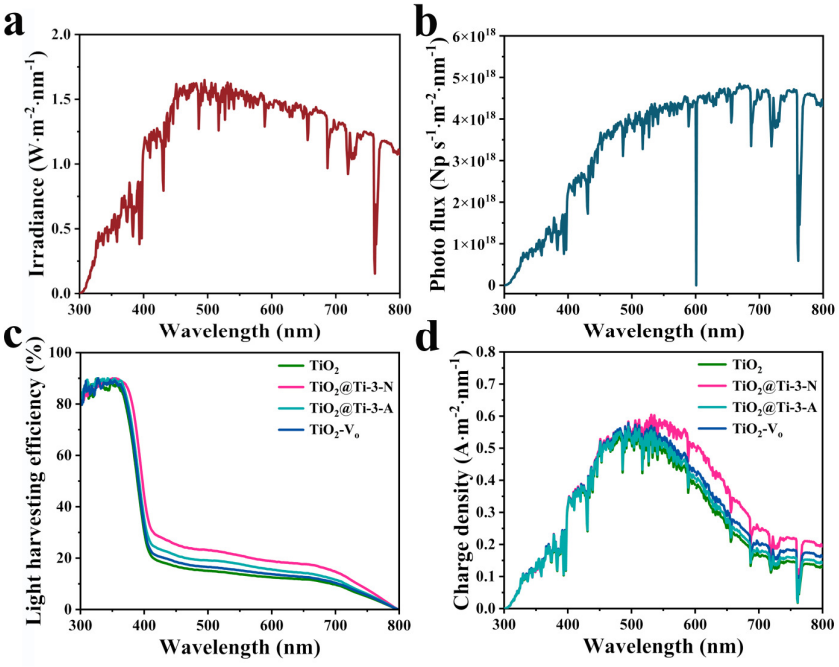

Fig. S12. (a) Original data of the full-spectrum light illumination spectral,[1] (named as "*E*", W·m^{-2}·nm^{-1}), (b) the photo flux (N_p), it was calculated from the full-spectrum light illumination spectrum (**Figure S13a**):[2]

$$N_p = \frac{E}{E_p} = \frac{E \times \lambda}{h \times c} \qquad (1)$$

where E_p is the energy of per photo (m^{-2}·s^{-1}·nm^{-1}), λ is the wavelength of light (nm), h is the planck constant (J·s), c is the lightspeed (m·s^{-1}).

(c) The light harvesting efficiencies (η_{LHE}) of TiO_2, TiO_2@Ti-3-N, TiO_2@Ti-3-A and TiO_2-V_o. η_{LHE} is converted from the UV–vis absorbance data (η_{abs}):[2]

$$\eta_{LHE} = (1 - 10^{-\eta abs}) \times 100\% \qquad (2)$$

(d) The charge density of TiO_2, TiO_2@Ti-3-N, TiO_2@Ti-3-A and TiO_2-V_o. It can be calculated from the photo flux N_p × light harvesting efficiency × e, where e is the electron charge (1.6022×10^{-19} C); the J_{abs} is the integration of charge density (A·m^{-2}·nm^{-1}) by wavelength (nm).

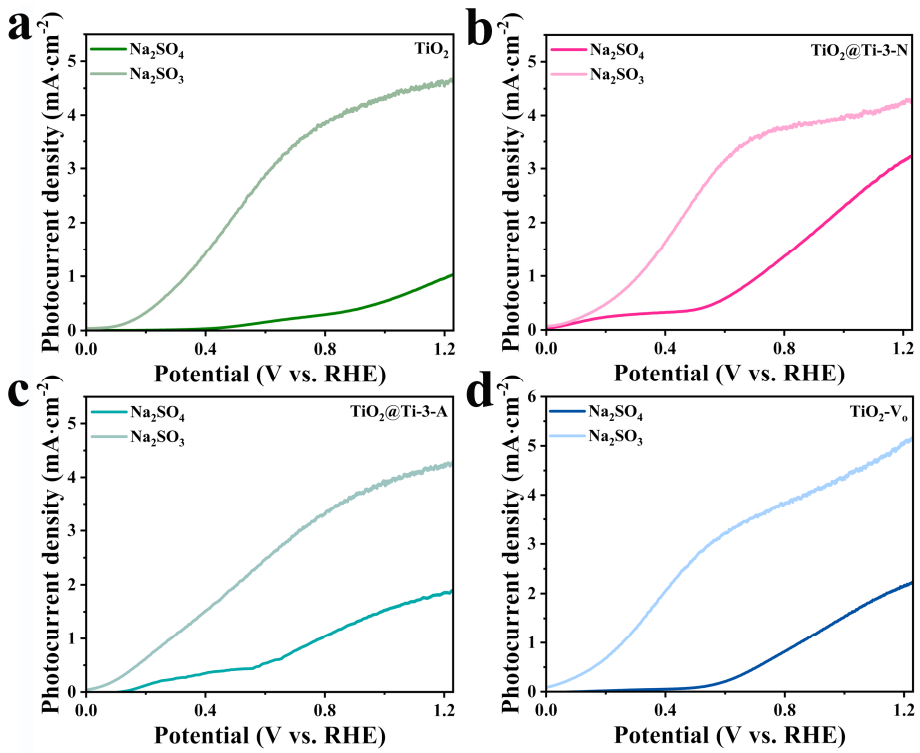

Fig. S13. LSV plots of photoanodes recorded under full-spectrum illumination (100 mW·cm^{-2}) in Na_2SO_4 and Na_2SO_3 electrolyte solutions: (a) TiO_2, (b) TiO_2@Ti-3-N, (c) TiO_2@Ti-3-A, and (d) TiO_2-V_o.

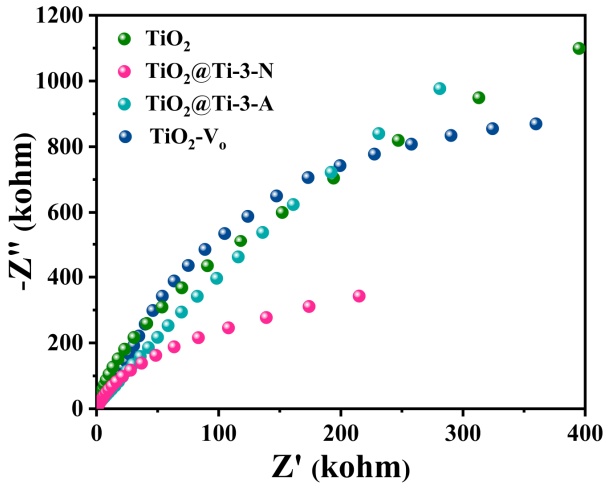

Fig. S14. Nyquist plots of TiO_2, TiO_2@Ti-3-N, TiO_2@Ti-3-A and TiO_2-V_o in dark.

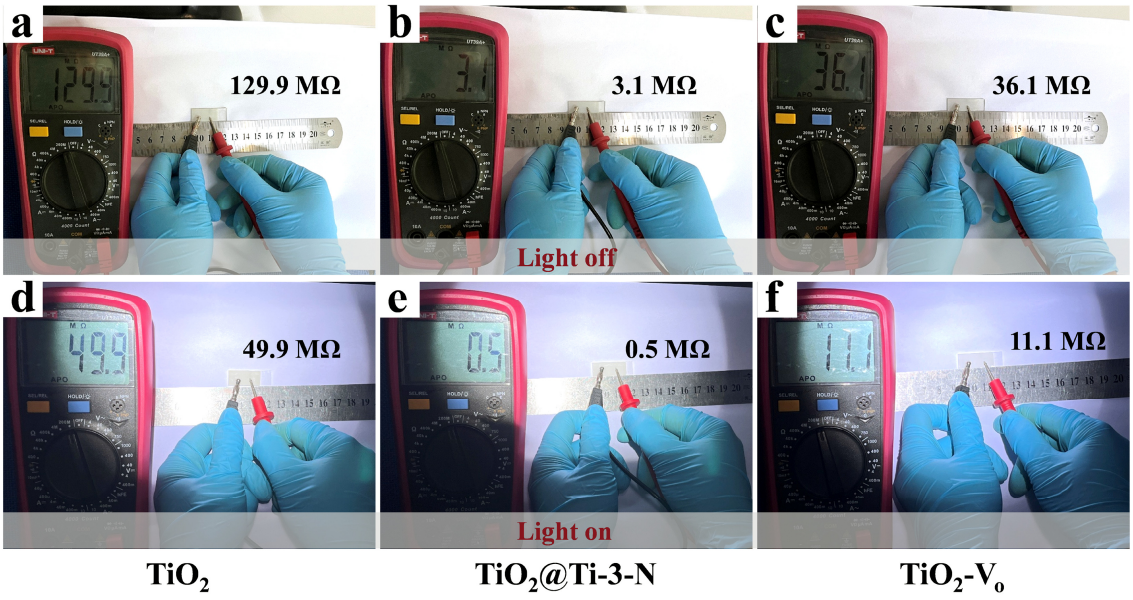

Fig. S15. Conductance of different TiO_2 photoanodes: (a, b, c) in the dark, and (d, e, f) under full-spectrum illumination (100 $mW \cdot cm^{-2}$).

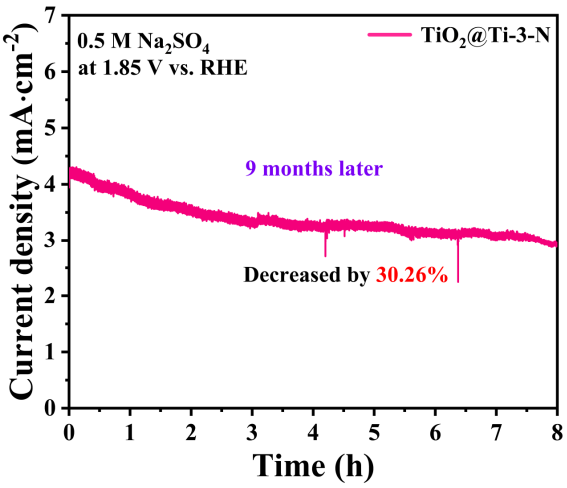

Fig. S16. Amperometric *J–t* curves of TiO_2@Ti-3-N photoanode measured at a bias of 1.85 V vs. RHE in Na_2SO_4 electrolyte solution after being stored at ambient condition for 9 months.

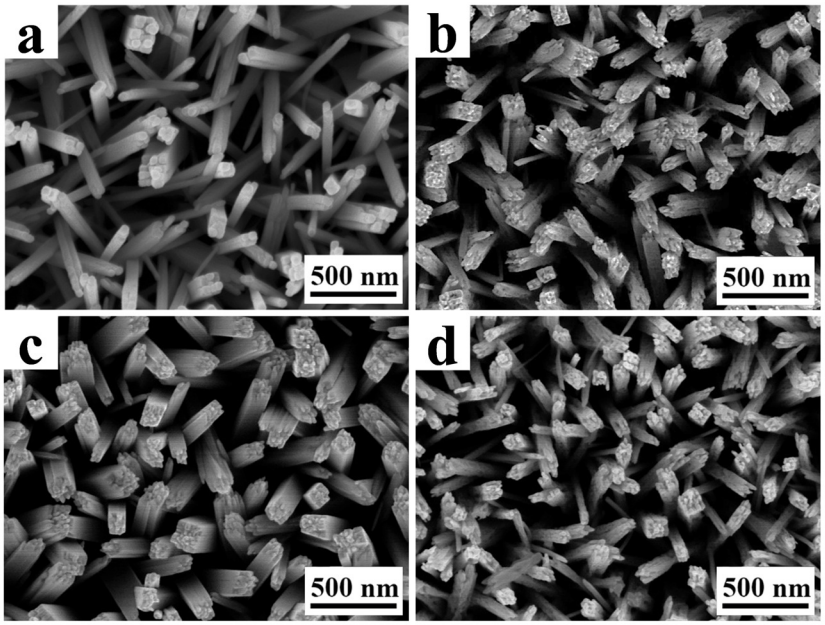

Fig. S17. SEM images of TiO_2 photoanodes before and after the PEC operation: (a) TiO_2@Ti-3-N, (b) TiO_2@Ti-3-N-used, (c) TiO_2-V_o, and (d) TiO_2-V_o-used.

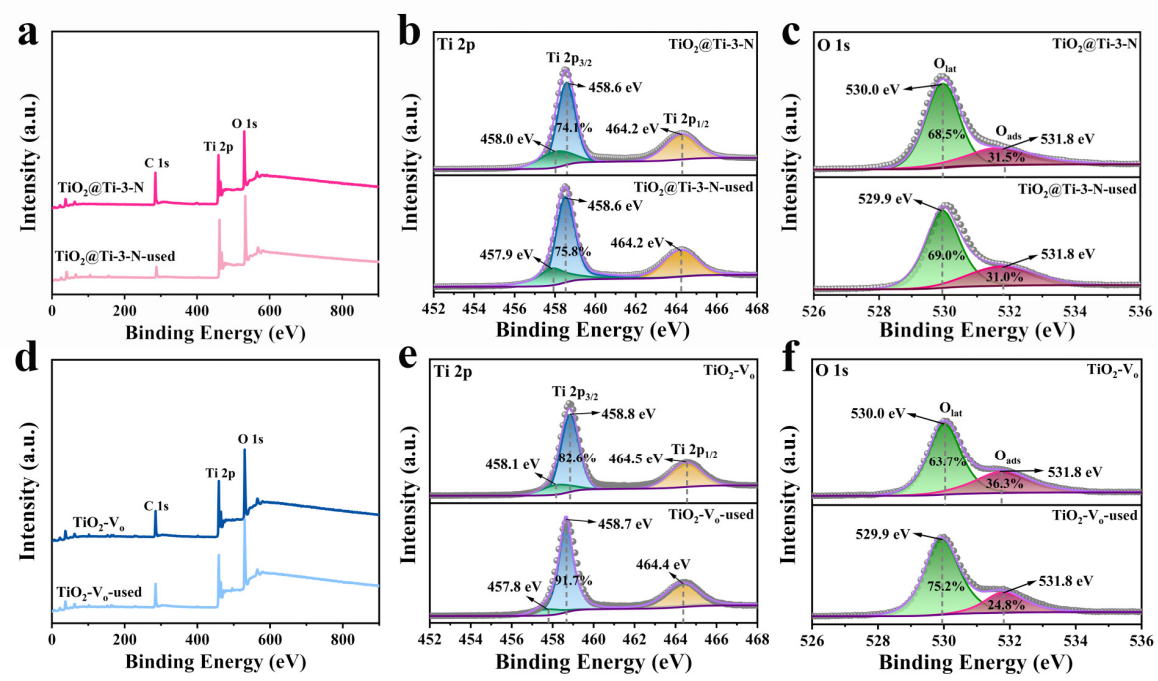

Fig. S18. XPS survey spectra (a) and high-resolution XPS spectra of Ti 2p (b) and O 1s (c) of TiO_2@Ti-3-N and TiO_2@Ti-3-N-used. XPS survey spectra (d) and high-resolution XPS spectra of Ti 2p (e) and O 1s (f) of TiO_2-V_o and TiO_2-V_o-used.

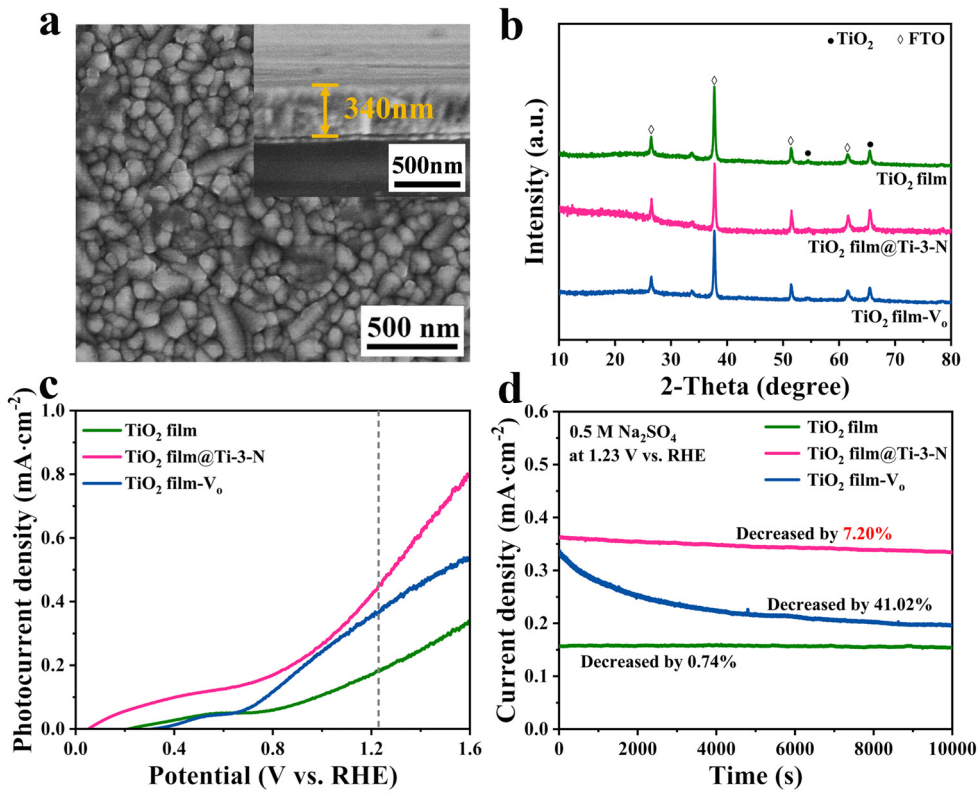

Fig. S19. (a) SEM image of TiO_2 film@Ti-3-N on FTO substrate; inset is a magnified cross-sectional view. (b) XRD patterns, (c) LSV curves recorded under full-spectrum illumination (100 mW·cm^{-2}), and (d) amperometric *J*–*t* curves of TiO_2 thin film, TiO_2 film@Ti-3-N and TiO_2 film-V_o.

Supplementary Tables

Table S1. Decay parameters (τ_1, τ_2, A_1 and A_2) and τ_{avg} of the TRPL decay curves of TiO_2 and TiO_2@Ti-3-N, where $\tau_{avg} = \frac{\sum A_i \tau_i^2}{\sum A_i \tau_i}$, i=1 and 2.[3]

Sample	τ_1 (ns)	τ_2 (ns)	A_1 (%)	A_2 (%)	τ_{avg} (ns)	χ^2
TiO_2	1.35	6.89	80.26	19.74	4.4	1.23
TiO_2@Ti-3-N	1.41	7.77	71.41	28.59	5.8	1.37

Table S2. R, C and τ calculations by fitting the circuit, where $\tau = R \times C$.[4]

Sample	R_1 (Ω)	C_{p1}	τ_1 (ms)	R_2 (Ω)	C_{p2}	τ_2 (ms)	χ^2 (10^{-4})
TiO_2	245.7	4.52E-6	1.11	1046.0	4.04E-4	422.6	11.3
TiO_2@Ti-3-N	72.6	4.15E-6	0.30	452.7	6.73E-4	304.7	8.9
TiO_2@Ti-3-A	42.6	4.13E-6	0.18	513.3	6.06E-4	311.1	6.5
TiO_2-V_o	134.5	4.32E-6	0.58	1124.3	5.16E-4	5801	10.7

Table S3. Comparison of PEC performance of TiO_2-based photoanodes by recently developed V_o generation methods and our approach.

Sample	Methods	Electrolyte	Electronic donor	Photocurrent density	Gas production	Stability evaluation
ΔV_o-TiO_2[5]	PEC-driven "self-purification" reconstruction	1 M NaOH	None	1.1 mA cm^{-2} at 1.23 V vs. RHE	H_2: 13 μmol h^{-1} cm^{-2} O_2: 6 μmol h^{-1} cm^{-2}	12 h
EBI TiO_2[6]	Electron-beam	1 M	None	1.5 mA cm^{-2} at	H_2: 27 μmol	10 h

	irradiation followed by loading of CoPi cocatalyst	NaOH		1.23 V vs. RHE	h^{-1} cm^{-2} O_2: 13 μmol h^{-1} cm^{-2}	
CR5[7]	Ce-doping treatment	0.1 M Na_2SO_4	None	1.98 mA cm^{-2} at 1.23 V vs. RHE	H_2: 37 μmol h^{-1} cm^{-2}	12 h
HV-TiO_2[8]	Annealing in high vacuum	0.5 M Na_2SO_4	None	2.02 mA cm^{-2} at 0.8 V vs. SCE	/	500 s
CQDs-H/TiO_2[9]	Surface Modification with carbon quantum dots (CQDs)	1 M KOH	None	3.0 mA cm^{-2} at 1.23 V vs. RHE	/	2 h
Ar-600[10]	Annealed at 600 ºC under Ar	1 M KOH	None	0.34 mA cm^{-2} at 1.23 V vs. RHE	H_2: 1.57 μmol h^{-1} cm^{-2}	/
V_o/Ti-Nb-O[11]	Electroreduced at 4 V for 5 min in 0.5 M Na_2SO_4	1 M KOH	None	1.72 mA cm^{-2} at 0 V vs. Ag/AgCl	/	3 h
TiO_2@Ti-3-N	Ti NEG coating and anaerobic annealing	0.5 M Na_2SO_4	None	2.2 mA cm^{-2} at 1.23 vs. RHE	H_2: 37.6 μmol h^{-1} cm^{-2} O_2: 18.3 μmol h^{-1} cm^{-2}	8 h & after 4-month storage in air

References

1. G173-03, A. S., Standard Tables for Reference Solar Spectral Irradiances: Direct Normal and Hemispherical on 37º Tilted Surface. *ASTM International*, *West Conshohocken*, *PA*, *(2003)* 2008.
2. S. Huo, Y. Wu, C. Zhao, F. Yu, J. Fang and Y. Yang, *Ind. Eng. Chem. Res.*, 2020, **59**, 14224−14233.

3. D. Pal, D. Mondal, D. Maity, D. De, M. K. Ganesha, A. K. Singh and G. G. Khan, *J. Mater. Chem. A*, 2023, **12**, 304.
4. Y. Han, J. Wu, Y. Li, X. Gu, T. He, Y. Zhao, H. Huang, Y. Liu and Z. Kang, *Appl. Catal. B: Environ.*, 2022, **304**, 120983.
5. K. H. Kim, C. W. Choi, S. Choung, Y. Cho, S. Kim, C. Oh, K. S. Lee, C. L. Lee, K. Zhang, J. W. Han, S. Y. Choi and J. H. Park, *Adv. Energy Mater.*, 2022, **12**, 2103495.
6. J. Huang, T. Chen, M. Zhao, P. Yi, F. Zhao, B. He, Y. Wang, Y. Chen, X. Liu and Z. Li, *CrystEngComm*, 2021, **23**, 2952–2960.
7. B.-L. Lin, R. Chen, M.-L. Zhu, A.-S. She, W. Chen, B.-T. Niu, Y.-X. Chen and X.-M. Lin, *Catalysts*, 2024, **14**, 639.
8. Y. Liu, F. Ren, S. Shen, J. Chen, Y. Fu, G. Cai, X. Wang, Z. Xing, L. Wu, X. Zheng and C. Jiang, *Int. J. Hydrogen Energy*, 2017, **43**, 2057–2063.
9. Z. Liang, H. Hou, Z. Fang, F. Gao, L. Wang, D. Chen and W. Yang, *ACS Appl. Mater. Interfaces*, 2019, **11**, 19167–19175.
10. Y. Son, R. Jung, J. Yoo and K. Lee, *Sol. RRL*, 2025, **9**, 2500334.
11. Z. Dong, J. Ma, D. Qin and S. Han, *Energy Fuels*, 2022, **37**, 592–603.